# Journal of Materials Chemistry C

Accepted Manuscript


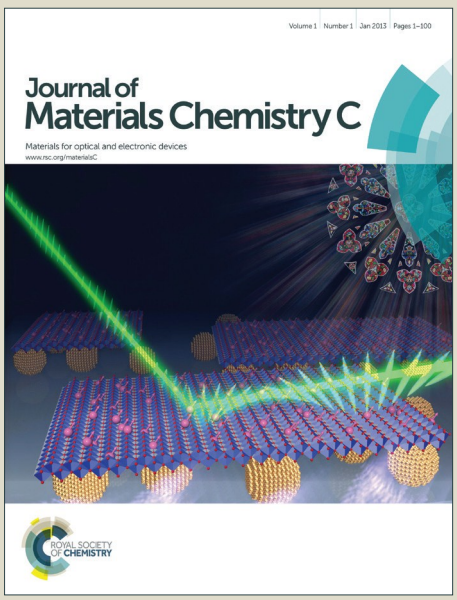





ROYAL SOCIETY OF CHEMISTRY

www.rsc.org/materialsC

# Eliminating Fermi-Level Pinning in PbS Quantum Dots using an Alumina Interfacial Layer

**Brian P. Bloom,[a] Madu N. Mendis,[a] Emil Wierzbinski and David H. Waldeck***

[a]*These authors contributed equally to this work*

*Department of Chemistry, University of Pittsburgh, Pittsburgh, Pennsylvania 15260*

*dave@pitt.edu

(412) 624-8430

## Abstract

Through a systematic approach we show that the insertion of a thin alumina layer in between a PbS QD layer and an Au substrate can eliminate Fermi level pinning. In this study band edge energies of different sized PbS QD monolayers with different cross-linkers were measured by using ultraviolet photoelectron spectroscopy and electrochemistry. When PbS QDs were immobilized directly on the Au, the measured valence band maximum was found to be insensitive to changes in the QD size or cross-linker indicating Fermi level pinning of the QD valence band to the Au Fermi level. After insertion of a thin film of alumina in between the PbS quantum dot monolayer film and the Au substrate, the measured valence band position revealed a shift that depended on ligand and QD size. These results identify a general method for eliminating Fermi level pinning in QDs and an approach for predictably controlling the energetics at the QD - metal interfaces which is beneficial for improving the performance of QD based solar cells.

## Introduction

Third generation solar cells are aimed at overcoming the thermodynamic limit set for the power conversion efficiency calculated by Shockley and Queisser in 1961 for a single junction and to do so at low-cost.[1,2] Several approaches have been proposed to exceed this limit and one of the most promising schemes is the multi exciton generation by semiconductor quantum dots (QDs). Compared to organic bulk heterojunction solar cells that suffer from lower carrier diffusion lengths and large offsets in the donor and acceptor levels, QD based solar cells have important advantages that mitigate these constraints. The optical band gap in the QDs can be

adjusted by changing their size, shape, surface passivation, and composition. Moreover, QDs allow for easy inexpensive solution based synthesis and processing, making them cost effective for large scale fabrication. In addition to these attributes, the organic ligand shell on a QD can be used to fine tune the electronic properties and the solvation characteristics.

In photovoltaic devices, QD films are commonly sandwiched between a cathode and an anode, which may be a metal (Schottky junction cells) or another semiconductor (p-n heterojunction solar cells), to form a complete functional device. Upon illumination by photons with sufficient energy, an electron-hole pair is formed in the QDs and they must be separated and extracted to opposing electrodes to produce a current. In a conventional p-n junction solar cell the charge carriers are driven by an electric field at the interface of the two semiconductors. One common strategy for enhancing charge separation is to alter the band positions within the QD films so that they form a staggered type-II alignment, creating a favorable energy cascade for both electron and hole transport.[3-5] Using arrays of different sized CdSe QDs, Weiss et al. have demonstrated that the photocurrent produced by each sized QD is largely dependent on the relative spatial arrangement and the band offset between them.[6] Similarly, El-Ballouli et al. have shown that favorable charge transfer from PbS QDs to PCBM[7] and cationic porphyrins[8] is determined by the size of the nanoparticle. In a previous study by Wang et al, donor- acceptor assemblies of CdSe-CdTe QD layers were shown to facilitate unidirectional charge transfer as long as proper energy band alignment is maintained in the photovoltaic device.[5] In a recent implementation of this strategy Chuang et al., used ligand induced band energy shifts to create a QD energy gradient that led to a photovoltaic efficiency over 8%.[3] Furthermore, an efficiency as high as 10.7% has been achieved by tuning the energy alignment at the rectifying interface, a new record for QD based solar cells.[9]

Surface ligands have been shown to shift the absolute energy positions of the valence band maximum (VBM) and conduction minimum (CBM) of QDs, and a growing body of evidence suggests that the magnitude of the energy shift can be characterized as a function of the dipole moment between the surface and linking group and the intrinsic dipole moment of the ligand itself. [10-12] By changing the capping ligand one can shift band energies of CdSe[10,13-15], CdS[16], PbS[4,11,17,18], as well as other nanocrystals[19]. Most recently, researchers have been using ligands to shift the absolute energy levels of QDs and to form an energy level gradient for

efficient charge separation. However, the magnitudes of the ligand's influence on the band energies can be affected by the electronic and chemical properties of a QD photovoltaic device at interfaces. When QDs are adsorbed onto a metal, charge equilibrium between the metal and the QD occurs; and it can 'pin' the electronic states of the QD to the Fermi level of the metal substrate. Often times the electronic energies of QDs determined in solution or under flat band conditions are used in determining a photovoltaic device architecture. When Fermi level pinning occurs in QD based solar cell devices, the QD size and ligand properties control over the energy position may no longer persist. In a study on CdSe QDs immobilized onto Au substrates by a decanedithiol linker, Markus et al. have shown that the absolute energy position of the VBM of the QDs larger than 2.8 nm does not change.[20] Depending upon the relationship of the QDs electronic states to that of the substrate, the CBM can also be pinned.[21] Previous electrochemical and UPS measurements on CdTe QD monolayers attached to an Au substrate through dithiol linkers showed no shift in VBM over the size range of 3.7 to 6.0 nm.[22] In Schottky junction solar cells, Fermi level pinning reduces the interfacial barrier height for charge injection and can reduce overall device efficiency. In some cases the pinning between the QDs and the electrode can persist for significant distances, e.g. 25 nm thick $MO_3$ layers.[23] Because the photoinduced free carriers must transfer through interfaces to be collected, control over the electronic properties of the QD-metal junction are important for improving the photoconversion efficiency of QD based solar cells.

## Background: Ligand effects on PbS QD Energetics

In photovoltaic devices, QDs are usually coated with short ligands to achieve better electronic coupling by changing the inter-QD tunneling distance and the effective dielectric constant. In a study by Liu et al, the dependence of ligand length and QD size on carrier mobility were reported for PbSe QDs field effect transistors.[24] The degree of QD surface passivation is also important for minimizing trap induced charge recombination. Wanger et al. showed that the effective density of trapped carriers has a strong dependence on ligand treatment in PbS QD films.[25] Zhitomirsky et al. measured the effect that QD films treated with organic (mercaptoproponoic acid) or a mixture of hybrid organic-inorganic (tetrabutylammonium iodide) ligand types have on charge mobility, trap density, and exciton diffusion length in QD films.[26] They have found that films with such organic-inorganic passivation exhibit the largest charge

diffusion lengths. These findings have led to the use of organic-inorganic hybrid passivation of PbS QDs to make a photovoltaic device with 7% power conversion efficiency.[27] Control of energetics at the rectifying interface of the PbS QD solar cells has allowed further improvement in photoconversion efficiency up to 10.7 %.

Axnanda et al. used photoelectron spectroscopy to measure the work function of 30 nm thick PbS QD films as a function of the capping ligand and observed a ligand effect on the energetics.[17] This work showed that methoxide, mercaptopropionic acid, and ethanedithiol (EDT) ligands could shift the VBM over a range of 0.3 eV. The resulting deeper VBM energy position has been explained by incomplete surface passivation and the presence of hole trap states. In a more comprehensive study, Brown et al. examined the band energies of PbS QD films (~100 nm) modified with 12 different ligands and reported that the VBM shifts over a range of 0.9 eV with ligand.[11] The same group has used the VBM energy offset between tetrabutylammonium iodide (TBAI) and 1, 2-ethanedithiol (EDT) capping ligands to alter the band energy positions and produce favorable charge transport in a photovoltaic device, achieving a power conversion efficiency of 8.5 %.[3] In another study by Crisp et al. it was shown that inorganic metal halide ligands in thick films of PbS (~ 300 -750 nm) leads to high efficiency photovoltaic devices.[18] They have used four different metal halides and attributed the improved device efficiency to better carrier transport in the film with halide passivation. Their XPS studies performed on the films of PbS treated with iodide ligands suggest a deeper work function, as compared to sulfur containing ligands. Santra et al. used three different para-substituted thiophenols with different dipole moments as capping ligands for PbS QD films (350 nm) to fabricate type-II heterojunction solar cells and reported a systematic shift in the VBM in PbS QDs.[4] Again type-II VBM alignment was shown to facilitate favorable unidirectional charge transport, however, when the bands edges are aligned in a way that the electron and hole encounter a potential barrier to reach the respective electrodes, a lower efficiency results.

Taken together, all the above studies affirm the role of capping ligand in manipulating the electronic band energies of PbS QDs and subsequently, the band alignment in solar cells. Control over the carrier mobility, trap state density, and charge diffusion has been achieved by tuning the cross-linker. Major advances in photoconversion efficiency have been obtained using this strategy in QD solar cell devices. Moreover, photovoltaic devices of PbS QD-polymer blends

(oly((4,8-bis(octyloxy)benzo(1,2-b:4,5-b′)-dithiophene-2,6diyl)(2((dodecyloxy)carbonyl)thieno(3,4-b)-thiophenediyl)) have reported a dependence of the open circuit voltage and overall device performance on the PbS QD ligand treatment which has been credited to the ligands influence over the carrier lifetime.[28] Despite these advances, the overall power conversion efficiencies of the QD based solar cells still remain below their expected performance largely because of low open circuit voltage.[29-32] Generally this limitation has been understood to originate from the presence of sub-bandgap states or midgap states that are formed by a large number of surface states associated with the defects on the QD surface. Such midgap states drive Fermi level pinning at the QD/metal interface in Schottky junction solar cells; as a result, the open circuit voltage is controlled by the pinning rather than the metal's work function or the QD's band edge.[31] This work is substantiated by the work of Yoon et al. who showed that insertion of an LiF layer between the top Al contact and PbS QDs improved the open circuit voltage in PbS QD solar cells.[33] Furthermore, oxidized interfacial layers on PbS QDs,[34] as well as insertion of a CdS shell on PbS QDs,[35] have been shown to increase the open circuit voltage in Schottky junction solar cell. A general approach to passivate these gap states and eliminate Fermi pinning at the QD – metal interfaces is not available.

PbS quantum dots (QDs) are promising candidates for third generation photovoltaics because the elements are earth abundant[36], the bandgap is tunable over a wavelength range that can best exploit the solar spectrum[37], and they offer the potential for multiple exciton generation[38,39]. This work examines the band edge energetics in PbS QD films and demonstrates the conditions for Fermi level pinning versus ligand control over the energetics. More specifically, this work shows that a thin alumina film (circa 1 to 3 nm) can be used to eliminate Fermi level pinning effects. The energy band positions of PbS QD monolayers on Au substrates, with and without an alumina layer, were measured using electrochemistry and ultraviolet photoelectron spectroscopy. When a monolayer of PbS QDs was deposited on top of an Au substrate, valence band positions were independent of known trends with QD size and surface ligand type, indicating strong Fermi level pinning. Introduction of a thin alumina interfacial layer between the Au and PbS inhibits Fermi level pinning so that the QD size and ligand can be used to manipulate the band edge positions. These findings highlight the importance of interfacial states in photovoltaic devices and enable precise control over QD properties for charge injection.

## Experimental

### Substrate Preparation

Substrates (12.5 mm × 25.0 mm) for these experiments were prepared by e-beam evaporation (AJA Deposition System) of 100 nm thick films of Au on glass substrates supported by a 5.0 nm Ti adhesion layer. For bare Au experiments the samples were plasma cleaned and used immediately. For experiments with an alumina layer, half of the substrate was covered with a wafer tape and poly-methyl-methacrylate (950k A11 PMMA, Micro Chem) was spun on it at a speed of 1500 rpm for 1 min using a spin processor (Laurell WS-400-6NPP-LITE). The wafer tape was removed, and the substrates were baked on a hot plate at 180 $^{o}$C for 5 min. Thin films of $Al_2O_3$ were then deposited using atomic layer deposition (Cambridge Nanotech Fiji). The samples were then kept overnight in acetone to remove the PMMA and to expose the underlying Au substrate on half of the electrode.

### PbS QD synthesis and characterization

The synthesis of PbS QDs followed a general procedure described elsewhere.[40] All of the materials, such as; $PbCl_2$ (Stern Chemicals), oleylamine (OLA, Sigma Aldrich), oleic acid (OA, Sigma Aldrich), and bis(trimethylsilyl) sulfide (TMS, Sigma Aldrich) were purchased in the highest purity grade available and used without further purification. In a typical synthesis, 3.0 mmol $PbCl_2$ (0.834 g) was mixed with 10 ml of OLA and degassed at 80.0 C, followed by heating to 140.0 C under argon. The suspension was maintained at this temperature for 30 min and then cooled to 30.0 C. Then 210.0 µl of TMS mixed in 2.0 ml of OLA was injected into the reaction mixture. The mixture was then rapidly elevated to a high temperature while stirring and subsequently quenched in a water bath once the desired QD size was obtained. The PbS QDs were precipitated from solution through the addition of acetone and centrifugation. The purified QDs were then dissolved in octane with 500 µl of OA, for ligand exchange, for 12 hours. The subsequent solution was then filtered using a 0.2 µm syringe filter, purified again, and then dissolved in 4.0 ml of octane.

Absorption spectra of the PbS QDs were recorded in octane using a spectrometer (Model 8453 Agilent Spectrometer). PbS QD emission spectra were obtained after exciting at 500 nm wavelength using a spectrofluorometer (Nanolog, Hobira).

**PbS Thin Film Preparation and Ligand Exchange**

All of the QD films were prepared by spin-casting. For each QD size, the PbS QD concentration was determined by evaluating the absorption spectrum. 10 μl of the PbS QD solution was spun onto Au substrates at a speed of 2500 rpm for 15 s. The resulting QD film was then cross-linked (*vide infra*) and the thickness was determined using AFM (Agilent Technologies) under tapping mode. This thickness was then used to determine a dilution factor of the QD solution to obtain a submonolayer thickness. The sample was prepared again and AFM was used to confirm submonolayer formation.

Ligands used for solid state ligand exchange, 1,4-benzedithiol (BDT, Alpha Aesar), 1,2-ethanedithiol (EDT, Sigma Aldrich), and ethylenediamine (EDA, Sigma Aldrich) were used as purchased. All ligands were dissolved in acetonitrile at varying concentrations; 1.7 mM BDT and one volume percent for both EDT and EDA. In a typical ligand exchange procedure, ~ 0.3 ml of ligand solution was dispersed onto the PbS monolayer film and allowed to sit for 1 min. The film was flushed with acetonitrile and spun dry two times to remove any unbound ligand. The samples were immediately transferred to a glove bag and stored under argon until electrochemical or UPS analysis.

**Atomic Force Microscopy Characterization**

AFM measurements were performed with an Agilent 5500 atomic force microscopy system using silicon cantilevers with resonance frequency of 96-175 kHz and spring constant of 5-37 N/m (PPP-SEIHR, Nanosensors). Precise values of the spring constants were determined using a thermal oscillation technique.[41] The film thickness was determined from the difference in the average height of the substrate covered with the PbS nanoparticle film and the bare gold substrate. The gold surface was exposed by scraping off the film in a 500 nm by 500 nm square area with a single AFM scan in contact mode with an applied load force of ca. 500 nN. Following this procedure, a larger 4 micrometer by 4 micrometer square area was imaged in acoustic AFM mode to capture the original nanoparticle film together with the exposed gold

substrate area. Switching between AFM operating modes was performed with a fully contracted z-axis piezoelement (the tip and the substrate were out of contact).

**Electrochemical Characterization**

Cyclic voltammetry on PbS films was performed in deoxygenated acetonitrile (99.9%, Sigma Aldrich) in a three electrode configuration on a CH Instruments 618B potentiostat. A Pt wire was used for the counter electrode, and $Ag/AgNO_3$ was used as the reference electrode. A 0.1 M solution of tetrabutylammonium hexafluorophosphate (Sigma Aldrich) was used as the supporting electrolyte. Voltammograms were obtained by scanning from 0 V to -1.2 V at a scan rate of 200 mV/s. The onset of the reduction peak for the QD was determined after subtraction of the background charging current, through an exponential fit. The formal potential of ferrocene / ferrocenium was used to calibrate the $Ag/AgNO_3$ reference electrode and convert the CBM of the PbS QDs to the vacuum energy scale.[22] The VBM was determined through addition of the optical band gap and exciton binding energy to the CBM.

**Photoemission Spectroscopy Characterization**

UPS measurements were performed using an ESCALAB 250XI XPS at a base pressure of $\sim 10^{-10}$ millibar. Electrical contact to the stage was made using copper tape on the edge of the Au substrate. Experiments were performed to ensure that no Cu photoemission signal contributed to the spectra. A bias of -5.0 eV was applied to the stage so that 1) the secondary electron cut off of the sample is distinguishable from that of the detector and 2) to ensure that the local vacuum level of the sample is more negative than that of the detector. A pass energy of 1.0 eV and a dwell time of >50 s were used to increase resolution and eliminate charging. A He (I) discharge lamp, 21.22 eV, was used as the ultraviolet source. The onset region and subsequent determination of the valence states were fit using previously published protocols.[20] In all experiments the Fermi edge of the underlying Au substrate is monitored to accurately reference the data.

## Results

Absorbance and emission spectra of the three different sized PbS quantum dots (QDs) used in this study are shown in Figure 1 (A). The sizes of these QDs were estimated from the empirical model developed by Moreels et al.[42] Note that the Stokes shift observed for the PbS

QDs changes with size in a manner consistent with previous literature.[43,44] The PbS QDs were then spin-coated onto an Au substrate and AFM measurements were performed. Figure 1 (B) and (C) show an example AFM image and measured thickness used to characterize each QD film for the determination of average thickness.

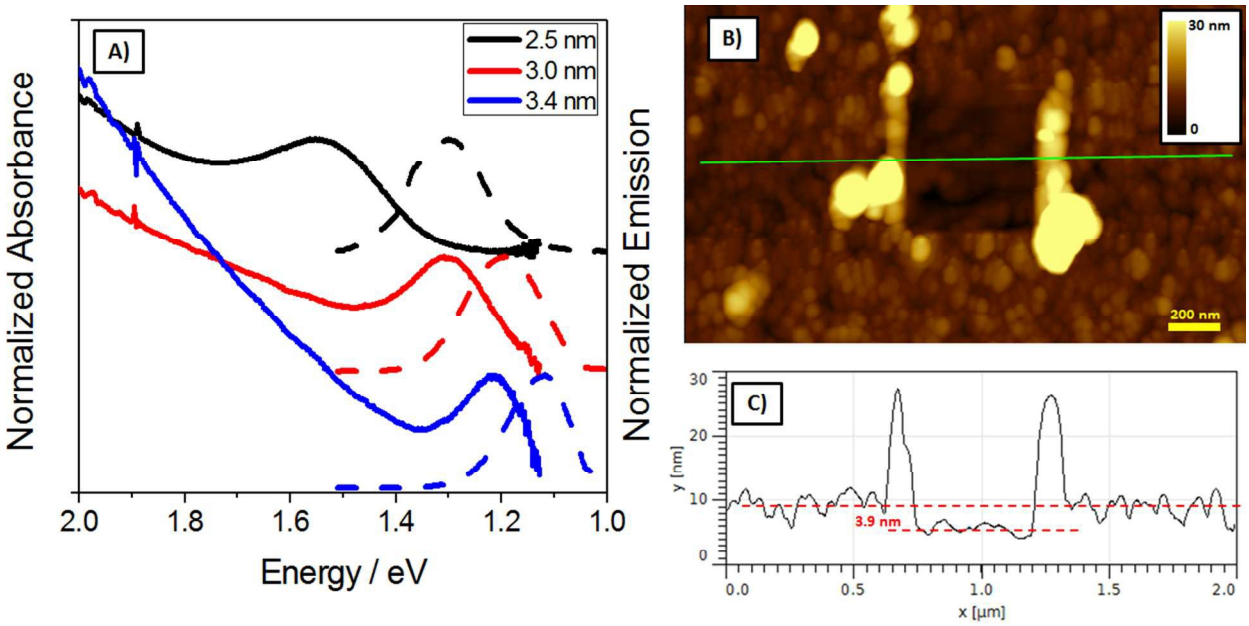


**Figure 1.** A) Normalized absorbance (solid line) and emission (dashed line) spectra of 2.5, 3.0, and 3.4 nm QDs in octane; B) AFM image of 3.0 nm PbS QDs that are cross-linked with EDT on Au; and C) height profile of the scratched QD film.

Figure 2 shows representative data from UPS (A) and electrochemistry (B) for 3.0 nm PbS with an EDA cross-linker. For UPS measurements, the VBM is determined by measuring the onset of the photoelectron spectra relative to the Fermi edge of Au ($E_f$). The work function of a bare Au substrate (4.8 eV) was then used to reference these data to the absolute electrode potential found in the electrochemical measurements. Cyclic voltammetry measurements on the CBM of PbS were performed in a manner similar to that reported previously.[22] Briefly, the PbS QDs exhibited a cathodic peak in the potential range of -0.9 to -0.5 volts versus Ag|AgNO$_3$, similar to those reported by Hyun et al.[45] Because the range overlaps with the limit of the solvent's potential window it was necessary to perform background subtraction. The voltammogram, excluding the peak region, was fit to an exponential (green) and then subtracted from the data to give a background subtracted (blue) curve, Figure 2B. This procedure minimizes

the effect of the capacitive current and allows for more accurate determination of the onset potential. Using the known absolute electrode potential for ferrocene, the onset potential can then be related to the vacuum energy scale by referencing to the ferrocene / ferrocenium redox couple.

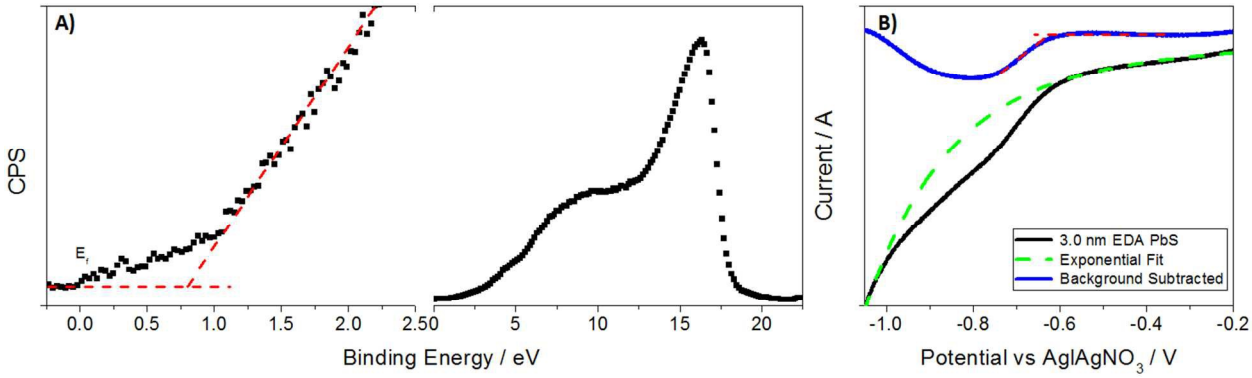


**Figure 2.** UPS spectra (A) and cyclic voltammogram (B) of 3.0 nm PbS QDs that are cross-linked by EDA to determine the VBM and CBM respectively. UPS of the onset region (A, left) and the full spectra (A, right) are shown. The red dashed line in both the UPS spectra and voltammogram show the onset potential associated with the corresponding electronic states.

Figure 3 summarizes the VBM and the CBM positions that were determined for thin films of the three different sized QDs that are capped with three different ligands: EDT, BDT, and EDA. The VBM was experimentally determined by UPS (Figure 3B, stars) and the CBM was experimentally determined using cyclic voltammetry (Figure 3A, stars). The optical bandgap and exciton binding energy were then used to determine the other bandedge. The measurements were performed on the same sample which was divided into two separate pieces using a glass cutter following the thin film fabrication. Each symbol represents the average of three independent measurements (an example of each is included in the supporting information). The standard deviation of the measurement is used for the error bars in the electrochemistry measurements and the resolution of the instrument, 0.1 eV, is used for the error bars in the UPS measurements. Slight differences in the electronic state positions obtained through the UPS and voltammetry methods exist and are attributed to environmental differences during measurement. Note that each of the experimental methods has limitations that affect the accuracy. The voltammetry is performed in an electrolyte solution where dielectric and double layer, as well as solvation, effects can influence the measured reduction potential. The UPS measurements are performed in vacuum and can be affected by local vacuum level shifts.[46] Despite the differences

in energy found for the VBM from the two different techniques the experimental data are in reasonable agreement. Moreover, the two methods independently demonstrate that the VBM of the PbS QD monolayer films does not change significantly over the size range and cross-linker types studied. In both experiments the CBM shifts systematically to higher energies with a decrease in QD size. For UPS measurements on medium and large sized QDs the CBM is reported below the bulk band energy of PbS (4.35 eV),[15] providing further evidence that Fermi-level realignment occurs at the metal-NP interface.

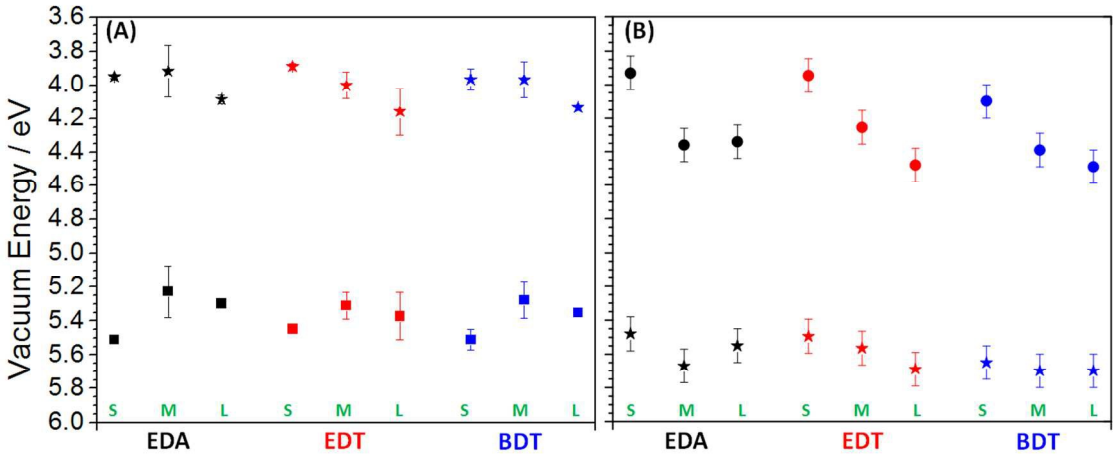


**Figure 3.** Electronic states of PbS monolayers determined by cyclic voltammetry (A) and photoelectron spectroscopy (B) are plotted versus the three different ligands used for cross-linking: EDA (black), EDT (red), and BDT (blue). Stars are representative of the experimentally determined values and a combination of the optical band gap and exciton binding energy was used to calculate the other bandedge. The S, M, and L represent the three different QD diameters 2.5 nm, 3.0 nm, and 3.4 nm, respectively. The dashed black line corresponds to the bulk CBM of PbS and the gray bar illustrates that all of the experimental UPS data fall within the error associated with the UPS measurement 5.6 +/- 0.1 eV. The error bars in the UPS measurement are a result of instrument resolution and the error bars in the electrochemistry data are representative of the standard deviation of multiple measurements.

When a thin interfacial layer of alumina is placed between the PbS monolayer film and the Au substrate, a trend different from that shown in Figure 3 was observed. The Au substrate used for these studies contained $Al_2O_3$ on one half of the substrate while the other half was bare Au (see Figure 4(A)). This procedure enabled a direct comparison of the two systems under identical conditions. UPS was employed to deduce the VBM for EDT cross-linked monolayer films of 2.5 nm and 3.0 nm diameter PbS QDs with 1 and 3 nm alumina layers (supporting

information Figure S4). Figure 4(B) shows the bandedge values obtained, as relative shifts from the Fermi level of Au ($E_f$), from these measurements. The plot shows that when no alumina is present (0 nm), no relative shift in VBM from the Fermi level of Au is found as a function of QD size. When alumina is present, however, the two different sized QDs have distinctly different electronic energy positions. Furthermore this shift depends on the thickness of the interfacial alumina, indicating that the PbS VBM is being decoupled from the Au Fermi level and the expected size dependent VBM shift is becoming manifest. Namely, the larger nanoparticles (in the 1 and 3 nm alumina thickness) have the VBM slightly higher, closer to that of bulk PbS. Note that a different cleaning procedure (see experimental section) was used here than in the previous measurements (Figure 3) in order to maintain the integrity of the film. As a result the work function of Au can shift slightly, however, both are internally consistent.

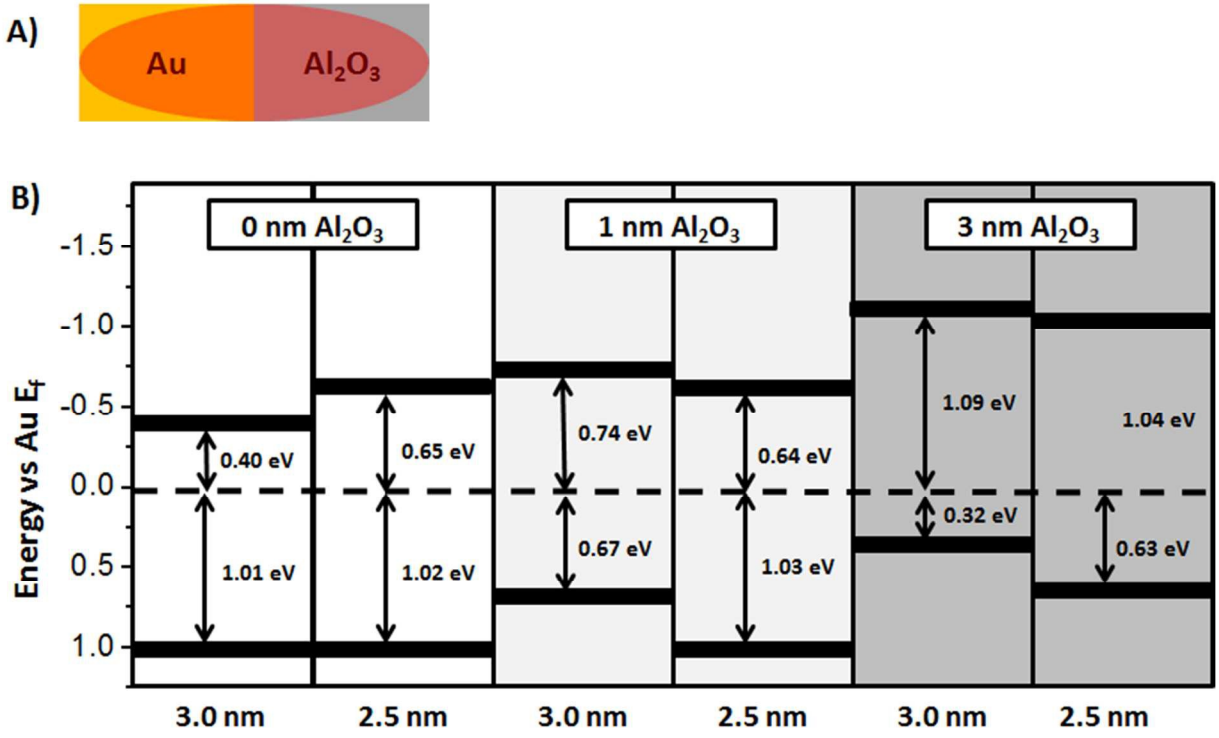


**Figure 4.** Diagram (A) shows a schematic of the substrate configuration used in this part of the study and diagram (B) shows the UPS determined energy band positions of the PbS monolayers. In B) the VBM and CBM are presented as relative shifts from the Au Fermi level ($E_f$ = 0 eV) for two different size QDs and three different thicknesses of alumina. The black boxes correspond to the band edge positions and their shift from $E_f$ is provided next to the double headed arrow.

Figure 5 shows the VBM and CBM of PbS QD monolayers on 100 nm Au substrates and their energies obtained by UPS for 2.5 nm QDs (open symbol) and 3.0 nm QDs (closed symbol) without (A) and with (B) a 3 nm alumina interfacial layer. The NPs are cross-linked in the same manner that was used in the Fermi level pinning study: BDT, EDT, and EDA. The energy of the VBM (black symbols) and CBM (red symbols) are reported with respect to the Au Fermi edge in the UPS spectra (supporting information Figure S5). On the Au substrate without alumina, it is clear that there is no variation in the VBM with QD diameter and cross-linker type. When alumina is present the VBM changes in a manner consistent with earlier reports: 1) the shift in VBM is correlated with the ligand identity for QDs of the same size and 2) the VBM shifts more strongly for QDs with a larger surface-to-volume ratio.

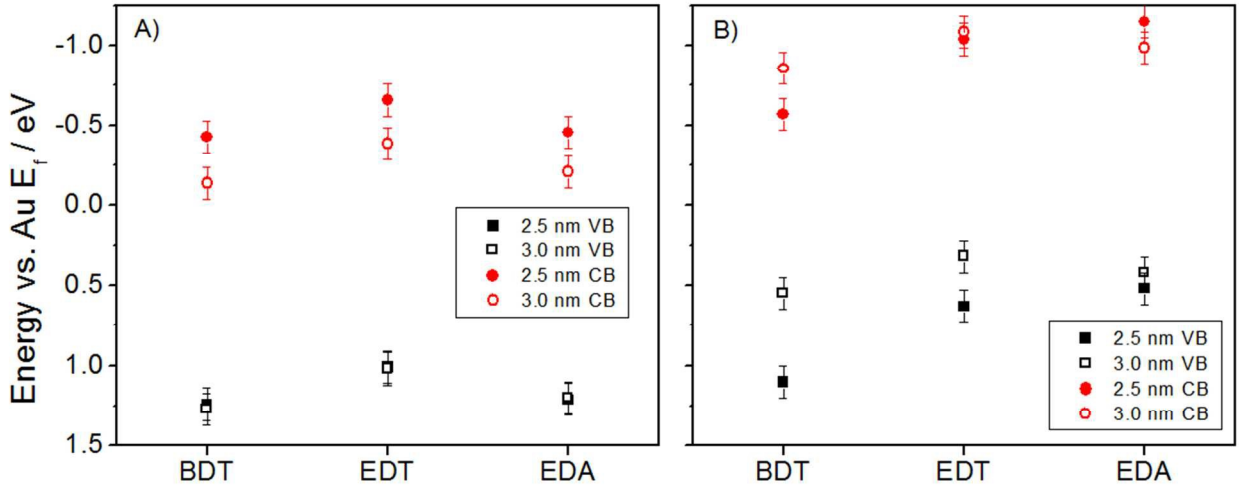


**Figure 5.** VBM (black symbols) and CBM (red symbols) of PbS monolayers with 2.5 nm (open symbols) and 3 nm (closed symbols) size QDs, as determined by UPS. Diagram A) is on the bare Au part of the substrate and diagram B) is for the part of the substrate covered with 3.0 nm of alumina. Three different cross-linkers were studied: BDT, EDT and EDA. Energy level positions are reported with respect to the Au Fermi edge in the UPS spectra.

## Discussion

When a semiconductor QD is in physical and electrical contact with a metal, charge equilibration occurs and the semiconductor's electronic states couple to those of the metal. If these interactions are caused by localized interfacial states,[47] then the charge exchange creates an electric field that 'pins' the semiconductor bandedge to the metal Fermi level. Which bandedge

is pinned depends on the details of the orbitals that contribute to the electronic coupling and the surface state energy, with respect to the bandedge. Fermi level pinning results in different sizes of QDs exhibiting similar barrier heights for charge injection upon photoexcitation. This phenomenon has been demonstrated for quantum dots at the interface with either a metal, or metal oxide, through electrochemical,[20,22] photoemission,[20-22,48-50] and Kelvin probe techniques.[51] The data in Figure 2 show that this pinning behavior is observed for monolayers of three differently sized PbS QDs on Au. Interestingly, the pinning effect persists for different cross-linkers (EDT, EDA, and BDT) despite recent studies which indicate that a change in the surface passivation changes bandedge positions of the QDs.

It is important to appreciate the difference between the monolayer films studied herein and the thicker films reported on by a number of other workers.[4,11,17] As the film thickness increases, the outer layers which are no longer directly coupled to the substrate, should have their energetics affected by the coupling between QDs, rather than by the asymmetric QD to metal coupling. In this limit, strong ligand dipolar effects are expected to determine the VBM and CBM of the PbS NPs. Thus one expects that the profile of bandedge energy with thickness will change through a thick film, from the Fermi level pinning value at the metal electrode surface to the QD-QD coupling value for thick films.

This study shows how the Fermi level pinning, caused by electronic interaction and/or charge exchange between the QDs surface states and the underlying metal electrode, can be eliminated by inserting a thin $Al_2O_3$ layer. The presence of this layer acts to reduce the metal-QD coupling and charge exchange; thereby inhibiting Fermi level pinning. As Figure 3 illustrates, an increase in the thickness of $Al_2O_3$ from 0 nm to 3 nm between Au and an EDT cross-linked PbS monolayer causes a shift in the VBM energy from a size independent pinned value to a size dependent value. These data provide direct evidence that strong coupling and charge displacement between the NPs and the Au electrode cause the Fermi level pinning, and ligand control is returned when this coupling is weakened enough. A different type of oxide film could be used to modulate the magnitude of the effect observed here; for example Beard et al. have examined how the open circuit voltage of a PbS QD film changes with thickness of a $MoO_3$ layer (up to 25 nm) between it and a metal electrode.[23] As such, it is expected that the barrier height for charge injection would be weakly dependent or even independent of cross-linker type or NP

size when the thickness of $MoO_3$ is less than this amount. The large thicknesses needed to reduce the pinning effect in their study likely arises because the electronic states of the $MoO_3$ are energetically close to the electronic states of PbS; ie. enhancing their mixing.

The system under investigation in Figure 4 is in agreement with the explanation given by Choi et al. in which a PbS film was annealed in air to passivate the NPs with a thin oxide layer prior to deposition of the top contact (LiF/Al/Ag).[34] The PbO passivates the surface state defects on the QDs that are assumed to participate in charge equilibration and therefore inhibits Fermi level pinning. In this situation, the Schottky barrier height for hole injection is expected to increase and the surface recombination is minimized, thus leading to an improvement in device photoconversion efficiency. Using a core-shell QD consisting of a CdS shell and PbS core has also been shown as a way to increase the open circuit voltage compared to core only devices of the same size, presumably for the same reason.[35] Deposition of a thin alumina film accomplishes the same goal as oxidation of the PbS and passivation with a CdS shell; namely, it inhibits charge equilibration at the interface, but unlike the other methods it also preserves the QD's chemical composition.

Shifts in the electronic state energies of the PbS QDs as a function of cross linker are also expected to return in the presence of an alumina tunneling barrier. Figure 5 shows how the VBM of 2.5 and 3.0 nm PbS QDs transition from ligand independent behavior on Au (a) to ligand dependent characteristic shifts, similar to those reported by Brown et al.[11], when alumina is present (b). Previous studies on CdSe have shown that small QDs exhibit larger ligand effects than large QDs because of their larger surface-to-volume ratio.[10] Figure 5(b) shows that BDT, EDT, and EDA cross-linkers shift the VBM much more for 2.5 nm PbS QDs than for 3.0 nm PbS QDs, in agreement with this claim. These ligand dependent shifts in electronic energies further corroborate the conclusion that the thin alumina layer acts to decouple the electronic states of QDs from Au. Operating under these conditions it should now be possible to tune the PbS QD properties at the interface and overcome charge injection and separation issues that have plagued previous architectures.

## Conclusion

This work demonstrates that Fermi level pinning persists in monolayer PbS QD films on Au substrates with different cross-linkers. Introduction of a thin alumina layer between the PbS QDs and the Au substrate was shown to weaken Fermi level pinning enough that size- and ligand-dependent properties are manifest. These findings point to a procedure for using ligand tuning of QD energetics to enhance charge injection and separation to overcome the open circuit voltage deficit reported for PbS.

## Author Information

Corresponding Author

*E-mail: dave@pitt.edu Tel.: (412) 624-8430

Note

The authors declare no competing financial interest.

## Acknowledgements

This work was funded by the U.S. Department of Energy (Grant No. ER46430). Brian P. Bloom is grateful for additional financial support from the R.K. Mellon foundation.

## References

(1) Brown, G. F.; Wu, J.: Third generation photovoltaics. *Laser & Photonics Reviews* **2009**, *3*, 394-405.

(2) Nozik, A. J.; Beard, M. C.; Luther, J. M.; Law, M.; Ellingson, R. J.; Johnson, J. C.: Semiconductor Quantum Dots and Quantum Dot Arrays and Applications of Multiple Exciton Generation to Third-Generation Photovoltaic Solar Cells. *Chemical Reviews* **2010**, *110*, 6873-6890.

(3) Chuang, C.-H. M.; Brown, P. R.; Bulović, V.; Bawendi, M. G.: Improved performance and stability in quantum dot solar cells through band alignment engineering. *Nat Mater* **2014**, *13*, 796-801.

(4) Santra, P. K.; Palmstrom, A. F.; Tanskanen, J. T.; Yang, N.; Bent, S. F.: Improving Performance in Colloidal Quantum Dot Solar Cells by Tuning Band Alignment through Surface Dipole Moments. *The Journal of Physical Chemistry C* **2015**, *119*, 2996-3005.

(5) Wang, Y.; Wang, L.; Waldeck, D. H.: Electrochemically Guided Photovoltaic Devices: A Photocurrent Study of the Charge Transfer Directionality between CdTe and CdSe Nanoparticles. *The Journal of Physical Chemistry C* **2011**, *115*, 18136-18141.

(6) Weiss, E. A.; Porter, V. J.; Chiechi, R. C.; Geyer, S. M.; Bell, D. C.; Bawendi, M. G.; Whitesides, G. M.: The Use of Size-Selective Excitation To Study Photocurrent through Junctions Containing Single-Size and Multi-Size Arrays of Colloidal CdSe Quantum Dots. *Journal of the American Chemical Society* **2008**, *130*, 83-92.

(7) El-Ballouli, A. a. O.; Alarousu, E.; Bernardi, M.; Aly, S. M.; Lagrow, A. P.; Bakr, O. M.; Mohammed, O. F.: Quantum Confinement-Tunable Ultrafast Charge Transfer at the PbS Quantum Dot and Phenyl-C61-butyric Acid Methyl Ester Interface. *Journal of the American Chemical Society* **2014**, *136*, 6952-6959.

(8) El-Ballouli, A. a. O.; Alarousu, E.; Kirmani, A. R.; Amassian, A.; Bakr, O. M.; Mohammed, O. F.: Overcoming the Cut-Off Charge Transfer Bandgaps at the PbS Quantum Dot Interface. *Advanced Functional Materials* **2015**, n/a-n/a.

(9) Kim, G.-H.; García de Arquer, F. P.; Yoon, Y. J.; Lan, X.; Liu, M.; Voznyy, O.; Yang, Z.; Fan, F.; Ip, A. H.; Kanjanaboos, P.; Hoogland, S.; Kim, J. Y.; Sargent, E. H.: High-Efficiency Colloidal Quantum Dot Photovoltaics via Robust Self-Assembled Monolayers. *Nano Letters* **2015**.

(10) Bloom, B. P.; Zhao, L.-B.; Wang, Y.; Waldeck, D. H.; Liu, R.; Zhang, P.; Beratan, D. N.: Ligand-Induced Changes in the Characteristic Size-Dependent Electronic Energies of CdSe Nanocrystals. *The Journal of Physical Chemistry C* **2013**, *117*, 22401-22411.

(11) Brown, P. R.; Kim, D.; Lunt, R. R.; Zhao, N.; Bawendi, M. G.; Grossman, J. C.; Bulović, V.: Energy Level Modification in Lead Sulfide Quantum Dot Thin Films through Ligand Exchange. *ACS Nano* **2014**, *8*, 5863-5872.

(12) Yang, S.; Prendergast, D.; Neaton, J. B.: Tuning Semiconductor Band Edge Energies for Solar Photocatalysis via Surface Ligand Passivation. *Nano Letters* **2012**, *12*, 383-388.

(13) Wang, C.; Shim, M.; Guyot-Sionnest, P.: Electrochromic Nanocrystal Quantum Dots. *Science* **2001**, *291*, 2390-2392.

(14) Wu, P.-J.; Tsuei, K.-D.; Hsieh, M.-T.; Wei, K.-H.; Liang, K. S.: Dependence of the final-state effect on the coupling between a CdSe nanoparticle and its neighbors studied with photoemission spectroscopy. *Physical Review B* **2007**, *75*, 115402.

(15) Jasieniak, J.; Califano, M.; Watkins, S. E.: Size-Dependent Valence and Conduction Band-Edge Energies of Semiconductor Nanocrystals. *ACS Nano* **2011**, *5*, 5888-5902.

(16) Shalom, M.; Rühle, S.; Hod, I.; Yahav, S.; Zaban, A.: Energy Level Alignment in CdS Quantum Dot Sensitized Solar Cells Using Molecular Dipoles. *Journal of the American Chemical Society* **2009**, *131*, 9876-9877.

(17) Axnanda, S.; Scheele, M.; Crumlin, E.; Mao, B.; Chang, R.; Rani, S.; Faiz, M.; Wang, S.; Alivisatos, A. P.; Liu, Z.: Direct Work Function Measurement by Gas Phase Photoelectron Spectroscopy and Its Application on PbS Nanoparticles. *Nano Letters* **2013**, *13*, 6176-6182.

(18) Crisp, R. W.; Kroupa, D. M.; Marshall, A. R.; Miller, E. M.; Zhang, J.; Beard, M. C.; Luther, J. M.: Metal Halide Solid-State Surface Treatment for High Efficiency PbS and PbSe QD Solar Cells. *Scientific Reports* **2015**, *5*, 9945.

(19) Soreni-Harari, M.; Yaacobi-Gross, N.; Steiner, D.; Aharoni, A.; Banin, U.; Millo, O.; Tessler, N.: Tuning Energetic Levels in Nanocrystal Quantum Dots through Surface Manipulations. *Nano Letters* **2008**, *8*, 678-684.

(20) Markus, T. Z.; Wu, M.; Wang, L.; Waldeck, D. H.; Oron, D.; Naaman, R.: Electronic Structure of CdSe Nanoparticles Adsorbed on Au Electrodes by an Organic Linker: Fermi Level Pinning of the HOMO. *The Journal of Physical Chemistry C* **2009**, *113*, 14200-14206.

(21) Markus, T. Z.; Itzhakov, S.; Alkotzer, Y. I.; Cahen, D.; Hodes, G.; Oron, D.; Naaman, R.: Energetics of CdSe Quantum Dots Adsorbed on TiO2. *The Journal of Physical Chemistry C* **2011**, *115*, 13236-13241.

(22) Wang, Y.; Xie, Z.; Gotesman, G.; Wang, L.; Bloom, B. P.; Markus, T. Z.; Oron, D.; Naaman, R.; Waldeck, D. H.: Determination of the Electronic Energetics of CdTe Nanoparticle Assemblies on Au Electrodes by Photoemission, Electrochemical, and Photocurrent Studies. *The Journal of Physical Chemistry C* **2012**, *116*, 17464-17472.

(23) Brown, P. R.; Lunt, R. R.; Zhao, N.; Osedach, T. P.; Wanger, D. D.; Chang, L.-Y.; Bawendi, M. G.; Bulović, V.: Improved Current Extraction from ZnO/PbS Quantum Dot Heterojunction Photovoltaics Using a MoO3 Interfacial Layer. *Nano Letters* **2011**, *11*, 2955-2961.

(24) Liu, Y.; Gibbs, M.; Puthussery, J.; Gaik, S.; Ihly, R.; Hillhouse, H. W.; Law, M.: Dependence of Carrier Mobility on Nanocrystal Size and Ligand Length in PbSe Nanocrystal Solids. *Nano Letters* **2010**, *10*, 1960-1969.

(25) Wanger, D. D.; Correa, R. E.; Dauler, E. A.; Bawendi, M. G.: The Dominant Role of Exciton Quenching in PbS Quantum-Dot-Based Photovoltaic Devices. *Nano Letters* **2013**, *13*, 5907-5912.

(26) Zhitomirsky, D.; Voznyy, O.; Hoogland, S.; Sargent, E. H.: Measuring Charge Carrier Diffusion in Coupled Colloidal Quantum Dot Solids. *ACS Nano* **2013**, *7*, 5282-5290.

(27) Ip, A. H.; Thon, S. M.; Hoogland, S.; Voznyy, O.; Zhitomirsky, D.; Debnath, R.; Levina, L.; Rollny, L. R.; Carey, G. H.; Fischer, A.; Kemp, K. W.; Kramer, I. J.; Ning, Z.; Labelle, A. J.; Chou, K. W.; Amassian, A.; Sargent, E. H.: Hybrid passivated colloidal quantum dot solids. *Nat Nano* **2012**, *7*, 577-582.

(28) Colbert, A. E.; Wu, W.; Janke, E. M.; Ma, F.; Ginger, D. S.: Effects of Ligands on Charge Generation and Recombination in Hybrid Polymer/Quantum Dot Solar Cells. *The Journal of Physical Chemistry C* **2015**, *119*, 24733-24739.

(29) Lan, X.; Masala, S.; Sargent, E. H.: Charge-extraction strategies for colloidal quantum dot photovoltaics. *Nat Mater* **2014**, *13*, 233-240.

(30) Gao, J.; Perkins, C. L.; Luther, J. M.; Hanna, M. C.; Chen, H.-Y.; Semonin, O. E.; Nozik, A. J.; Ellingson, R. J.; Beard, M. C.: n-Type Transition Metal Oxide as a Hole Extraction Layer in PbS Quantum Dot Solar Cells. *Nano Letters* **2011**, *11*, 3263-3266.

(31) Luther, J. M.; Law, M.; Beard, M. C.; Song, Q.; Reese, M. O.; Ellingson, R. J.; Nozik, A. J.: Schottky Solar Cells Based on Colloidal Nanocrystal Films. *Nano Letters* **2008**, *8*, 3488-3492.

(32) Chuang, C.-H. M.; Maurano, A.; Brandt, R. E.; Hwang, G. W.; Jean, J.; Buonassisi, T.; Bulović, V.; Bawendi, M. G.: Open-Circuit Voltage Deficit, Radiative Sub-Bandgap States, and Prospects in Quantum Dot Solar Cells. *Nano Letters* **2015**, *15*, 3286-3294.

(33) Yoon, W.; Boercker, J. E.; Lumb, M. P.; Placencia, D.; Foos, E. E.; Tischler, J. G.: Enhanced Open-Circuit Voltage of PbS Nanocrystal Quantum Dot Solar Cells. *Scientific Reports* **2013**, *3*, 2225.

(34) Choi, M.-J.; Oh, J.; Yoo, J.-K.; Choi, J.; Sim, D. M.; Jung, Y. S.: Tailoring of the PbS/metal interface in colloidal quantum dot solar cells for improvements of performance and air stability. *Energy & Environmental Science* **2014**, *7*, 3052-3060.

(35) Speirs, M. J.; Balazs, D. M.; Fang, H. H.; Lai, L. H.; Protesescu, L.; Kovalenko, M. V.; Loi, M. A.: Origin of the increased open circuit voltage in PbS-CdS core-shell quantum dot solar cells. *Journal of Materials Chemistry A* **2015**, *3*, 1450-1457.

(36) Wadia, C.; Alivisatos, A. P.; Kammen, D. M.: Materials Availability Expands the Opportunity for Large-Scale Photovoltaics Deployment. *Environmental Science & Technology* **2009**, *43*, 2072-2077.

(37) Graetzel, M.; Janssen, R. A. J.; Mitzi, D. B.; Sargent, E. H.: Materials interface engineering for solution-processed photovoltaics. *Nature* **2012**, *488*, 304-312.

(38) Ellingson, R. J.; Beard, M. C.; Johnson, J. C.; Yu, P.; Micic, O. I.; Nozik, A. J.; Shabaev, A.; Efros, A. L.: Highly Efficient Multiple Exciton Generation in Colloidal PbSe and PbS Quantum Dots. *Nano Letters* **2005**, *5*, 865-871.

(39) Yang, Y.; Rodríguez-Córdoba, W.; Lian, T.: Multiple Exciton Generation and Dissociation in PbS Quantum Dot-Electron Acceptor Complexes. *Nano Letters* **2012**, *12*, 4235-4241.

(40) Zhang, J.; Gao, J.; Miller, E. M.; Luther, J. M.; Beard, M. C.: Diffusion-Controlled Synthesis of PbS and PbSe Quantum Dots with in Situ Halide Passivation for Quantum Dot Solar Cells. *ACS Nano* **2014**, *8*, 614-622.

(41) Hutter, J. L.; Bechhoefer, J.: Calibration of atomic-force microscope tips. *Review of Scientific Instruments* **1993**, *64*, 1868-1873.

(42) Moreels, I.; Lambert, K.; Smeets, D.; De Muynck, D.; Nollet, T.; Martins, J. C.; Vanhaecke, F.; Vantomme, A.; Delerue, C.; Allan, G.; Hens, Z.: Size-Dependent Optical Properties of Colloidal PbS Quantum Dots. *ACS Nano* **2009**, *3*, 3023-3030.

(43) Peterson, J. J.; Krauss, T. D.: Photobrightening and photodarkening in PbS quantum dots. *Physical Chemistry Chemical Physics* **2006**, *8*, 3851-3856.

(44) Zhang, J.; Jiang, X.: Confinement-Dependent Below-Gap State in PbS Quantum Dot Films Probed by Continuous-Wave Photoinduced Absorption. *The Journal of Physical Chemistry B* **2008**, *112*, 9557-9560.

(45) Hyun, B.-R.; Zhong, Y.-W.; Bartnik, A. C.; Sun, L.; Abruña, H. D.; Wise, F. W.; Goodreau, J. D.; Matthews, J. R.; Leslie, T. M.; Borrelli, N. F.: Electron Injection from Colloidal PbS Quantum Dots into Titanium Dioxide Nanoparticles. *ACS Nano* **2008**, *2*, 2206-2212.

(46) Munro, A. M.; Zacher, B.; Graham, A.; Armstrong, N. R.: Photoemission Spectroscopy of Tethered CdSe Nanocrystals: Shifts in Ionization Potential and Local Vacuum Level As a Function of Nanocrystal Capping Ligand. *ACS Applied Materials & Interfaces* **2010**, *2*, 863-869.

(47) Tung, R. T.: Formation of an electric dipole at metal-semiconductor interfaces. *Physical Review B* **2001**, *64*, 205310.

(48) Xie, Z.; Markus, T. Z.; Gotesman, G.; Deutsch, Z.; Oron, D.; Naaman, R.: How Isolated Are the Electronic States of the Core in Core/Shell Nanoparticles? *ACS Nano* **2011**, *5*, 863-869.

(49) Carlson, B.; Leschkies, K.; Aydil, E. S.; Zhu, X. Y.: Valence Band Alignment at Cadmium Selenide Quantum Dot and Zinc Oxide (10$\bar{1}$0) Interfaces. *The Journal of Physical Chemistry C* **2008**, *112*, 8419-8423.

(50) Timp, B. A.; Zhu, X. Y.: Electronic energy alignment at the PbSe quantum dots/ZnO(10$\bar{1}$0) interface. *Surface Science* **2010**, *604*, 1335-1341.

(51) Gao, J.; Luther, J. M.; Semonin, O. E.; Ellingson, R. J.; Nozik, A. J.; Beard, M. C.: Quantum Dot Size Dependent J−V Characteristics in Heterojunction ZnO/PbS Quantum Dot Solar Cells. *Nano Letters* **2011**, *11*, 1002-1008.

## Cover Graphic